ACS Photonics
Article
pubs.acs.org/journal/apchd5

Slow Down of Charge Transfer Owing to Auger Recombination and Two-Photon Action Cross-Section of CdS−CdSe−CdS Segmented Nanorods

Radhu Subha,[†,§] Venkatram Nalla,[†,∥] Eugene J. Q. Lim,[‡] Cherianath Vijayan,[§] Barry B. S. Huang,[‡] Wee Shong Chin,[‡] and Wei Ji*,[†]

[†]Department of Physics, Faculty of Science, National University of Singapore, 2 Science Drive 3, 117542, Singapore
[‡]Department of Chemistry, Faculty of Science, National University of Singapore, 3 Science Drive 3, 117543, Singapore
[§]Department of Physics, Indian Institute of Technology, Madras, Chennai, India, 600036
[∥]Centre for Disruptive Photonic Technologies, Nanyang Technological University, 637371, Singapore

Ⓢ *Supporting Information*

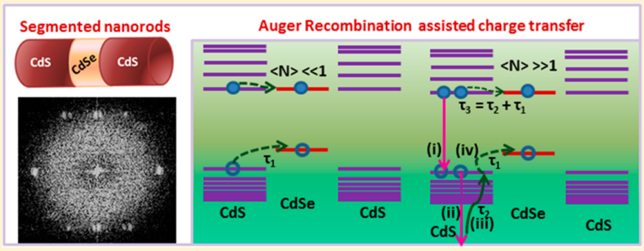

ABSTRACT: We report on the dynamical properties of photoexcited carriers, particularly the charge transfer, in CdS−CdSe−CdS segmented nanorods using femtosecond transient pump−probe spectroscopy. Design of this kind of heteronanostructures with the possibility of variation of the relative volumes of CdS and CdSe segments permits independent tuning of one-photon and two-photon absorption cross-sections over a wide range of wavelengths, with specific advantages in applications related to photovoltaics and multiphoton microscopy. Intensity-dependent charge transfer dynamics in CdS−CdSe−CdS segmented nanorods indicates that the rate of charge transfer from CdS to CdSe is influenced by the number of electron−hole pairs generated in the nanorod. We attribute this change in the rate constant to Auger recombination-assisted charge transfer, which becomes the predominant relaxation mechanism at high intensities. Charge transfer also results in a large two-photon absorption cross-section, on the order of 10^4 GM (1 GM = 10^{-50} cm^4 s photon^{-1}), at 1.55 eV in these heteronanostructures. Furthermore, two-photon absorption induced photoluminescence on near-infrared excitation (1.55−0.99 eV) suggests that the local field effects plays a role in determining the effective two-photon action cross-section of heteronanostructures, offering a platform for engineering optical nonlinearity.

KEYWORDS: *nonlinear optics, CdS, CdSe, charge transfer, Auger recombination, two-photon absorption, nanorod, heterostructure*

Semiconductor heteronanostructures have great potential in a broad range of applications such as lasing, light-emitting, and photovoltaic devices because of their high photoluminescence (PL) quantum yields with spectrally narrow and symmetric emission, suppressed Auger recombination, and significantly suppressed blinking and photobleaching.[1−6] Heteronanostructures of CdS−CdSe are particularly interesting among various heterojunction nanomaterials studied so far, such as CdTe/CdS,[7] CdSe/ZnS,[8] ZnSe/CdSe,[9] CdS/ZnSe,[10] and CdS/CdSe core−shell nanostructures,[1,11] dot-in-rod nanostructures,[12,13] tetrapods,[14] octapods,[15,16] and dot-in-plate.[17] This is because they possess (1) relatively low lattice mismatch, leading to a lower defect density and thus high PL quantum yield up to 97%;[1] (2) longer biexciton lifetimes up to nanoseconds; (3) biexciton quantum yields of 40−50% reported in CdS−CdSe core−shell structures;[2] and (4) band alignment that is tunable from type I to quasi-type II by varying the core size, rod size, interfacial strain, etc.[18] With quasi-type II alignment and efficient charge transfer from CdS to CdSe, CdS−CdSe tetrapods and dot-in-rod structures are suggested to be suitable candidates for photovoltaic applications.[19,20]

While the band alignment of quasi-type II in CdS−CdSe heteronanostructures favors the charge separation and collection, the one-photon absorption cross-section below 2.4 eV in these nanostructures is limited by the volume of CdSe, which is used in the form of a quantum dot (QD) in the reported heteronanostructures such as core−shell, dot-in-rod, and tetrapod. One of the feasible strategies to achieve higher absorption cross-sections over a wide range of wavelengths in CdS−CdSe heteronanostructures is by replacing CdSe QDs with nanorods since the latter have a larger absorption cross-section, enhanced stabilities, and linearly polarized emission compared to QDs.[21,22] In this work, we report on our investigation into charge transfer mechanisms in segmented-nanorod heterostructures, which offers control of the absorption cross-section over a wide range of wavelengths.

Optical excitation of a semiconductor with photons of energy higher than the band gap leads to the generation of

Received: April 6, 2014
Published: December 8, 2014

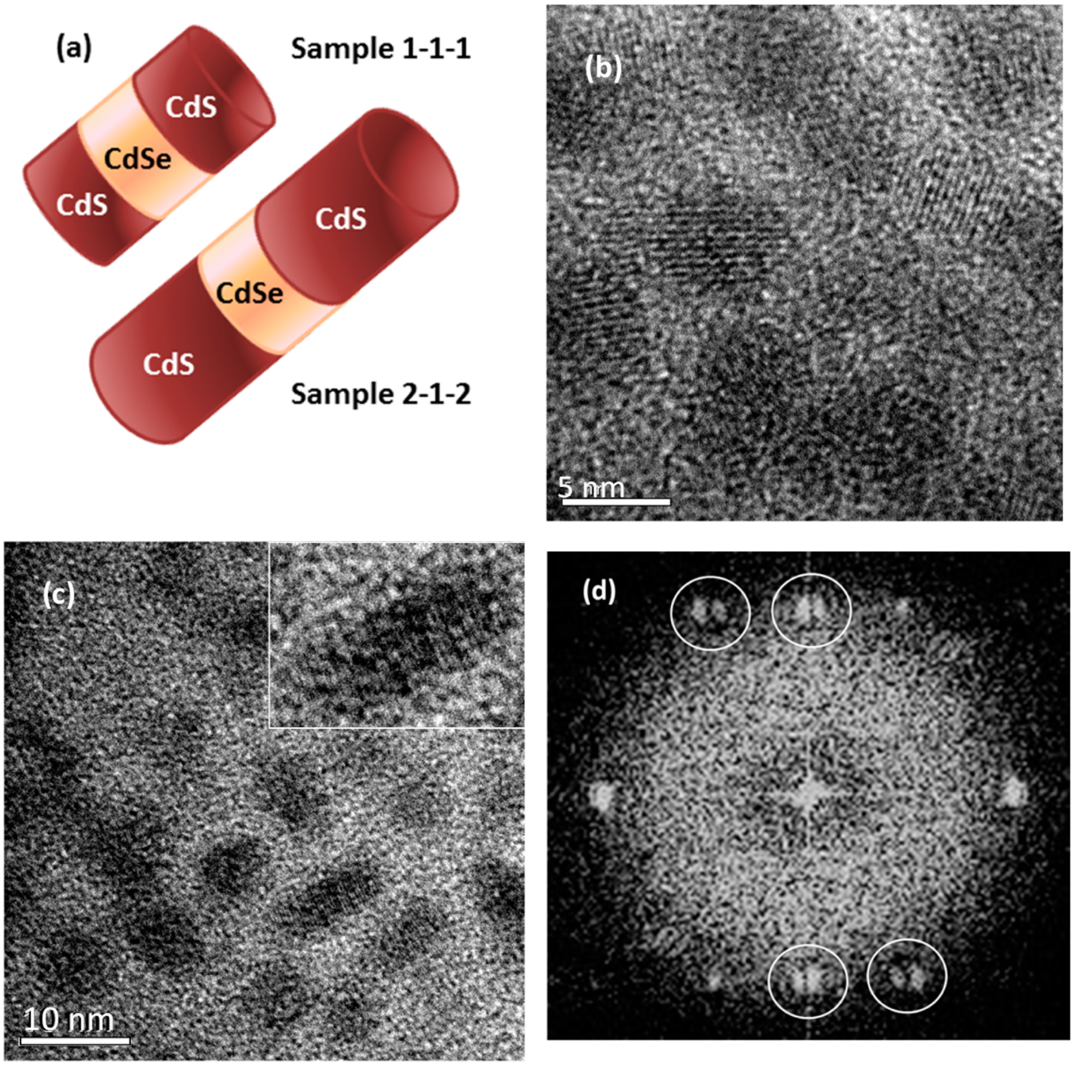

Figure 1. (a) Schematic structure of the CdS−CdSe−CdS segmented nanorods. (b and c) HRTEM images of the CdS−CdSe−CdS segmented nanorods for sample 1-1-1 (b) and sample 2-1-2 (c). Inset in (c): HRTEM image clearly showing lattice fringes of one rod. (d) SAED pattern of the CdS−CdSe−CdS reveals pairs of diffraction peaks along different lattice directions (marked with circles), indicating distinct lattices of CdS and CdSe inside one nanorod.

nonequilibrium carrier densities.[23] The optically excited carriers undergo spatial and temporal evolution to reach thermal equilibrium with the lattice with characteristic time that depends on different relaxation mechanisms.[24] In CdS−CdSe heteronanostructures, charge transfer from CdS to CdSe was reported to be a prominent relaxation mechanism of the optically excited carriers in CdS−CdSe heteronanostructures.[25,26] A recent report indicated that Coulombic interaction between the electrons and holes in CdS−CdSe tetrapods leads to coupled electron−hole transfer from CdS to CdSe.[27] Using a transient pump−probe spectroscopic technique, Wu et al. demonstrated that the localization of holes in CdS−CdSe dot-in-rod nanostructures leads to the formation of three spatially separated long-lived exciton states.[20] Understanding the photoexcited carrier dynamics in CdS−CdSe heteronanostructures is the key to utilizing these heteronanostructures in technological applications, since the switching speed and efficiency of nanoscale devices based on heteronanostructures could be influenced by the rate of charge transfer of optically excited carriers. While the carrier dynamics has been explored in these heteronanostructures at low intensity, only a few reports are available on the intensity dependence of the charge transfer in these systems.[25,28] Increasing the pump intensity generates more carriers, and these carriers are spatially confined within the dimensions of nanorods, leading to increased carrier−carrier interactions, such as Auger recombination in nanomaterials.[29] Achermann et al. reported that the intraband relaxation in CdSe nanorods gets delayed at high intensities as a result of Auger recombination,[30] but the effect of Auger recombination on charge transfer has not been systematically investigated yet. Here, we focus on this aspect, particularly on charge transfer rate from CdS to CdSe in the two excitation regimes: (1) $\langle N\rangle \ll 1$ and (2) $\langle N\rangle \gg 1$ where $\langle N\rangle$ is defined as the average number of photoexcited electron−hole pairs per segmented nanorod.

Furthermore, efficient charge transfer from CdS to CdSe leads to high PL quantum yields in CdS−CdSe heteronanostructures. Recently CdS−CdSe core−shell nanostructures was regarded as superior *in vivo* imaging agents compared to conventional QDs for bioimaging in multiphoton microscopy.[1] CdS−CdSe dot-in-rod structures were found to be a suitable candidate for low-threshold lasers by two-photon absorption at

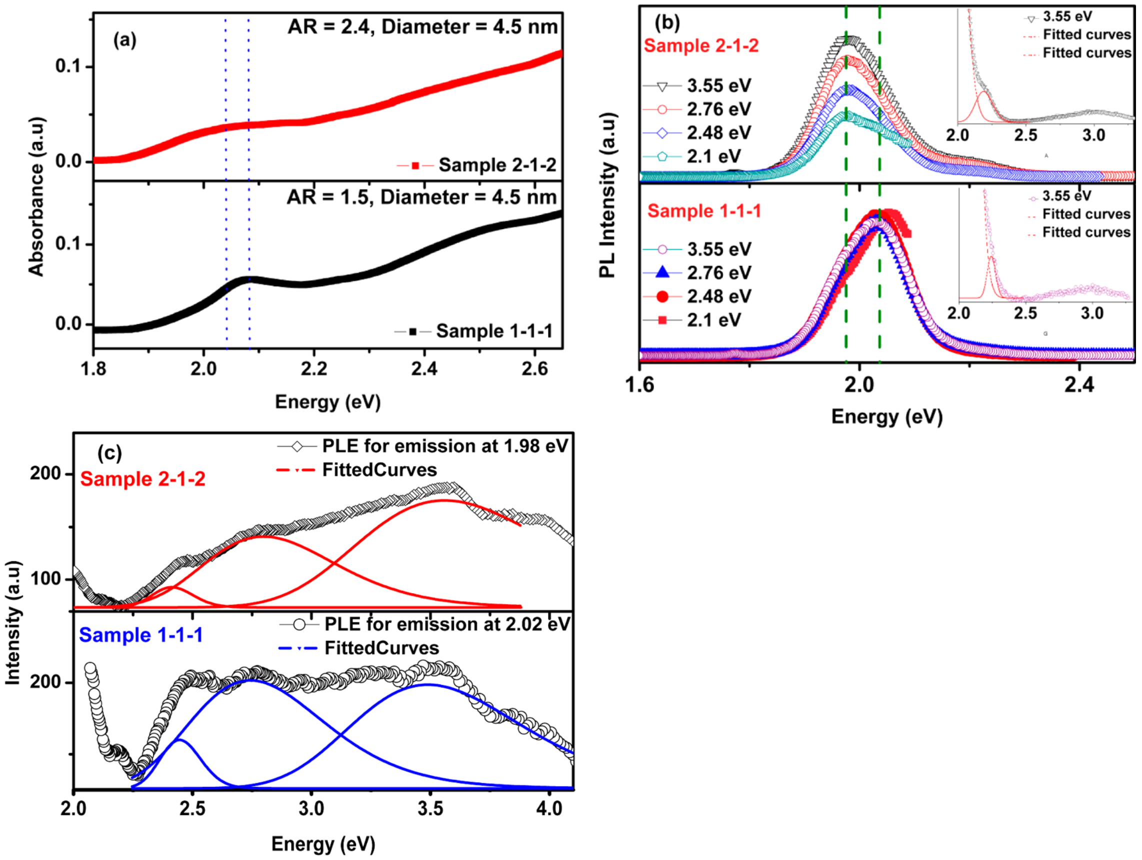

Figure 2. Optical properties of CdS−CdSe−CdS segmented nanorods. (a) UV−visible absorption spectra of sample 2-1-2 (top, red) and sample 1-1-1 (bottom, black). (b) PL emission spectra showing emission peaks at 1.98 and 2.02 eV for sample 2-1-2 and sample 1-1-1, respectively, at varying excitation energy. Insets show the enlarged view of the observed weak emission in the CdS segment of the nanorod in the energy range 2−3.2 eV. (c) PL excitation spectra (PLE) showing wavelength-dependent emission for sample 2-1-2 (top) and sample 1-1-1 (bottom).

1.55 eV (800 nm).[31] A large two-photon absorption cross-section on the order of 10^4−10^5 GM at 800 nm was also observed in CdS−CdSe heteronanostructures.[31,32] Note that, in these reports, the two-photon absorption studies are limited to 1.55 eV. Excitation in the NIR-II window (1.2−0.92 eV) can enhance the penetration depth of the incident photons, particularly in deep tissue imaging, making use of the lower scattering and autofluorescence in biological tissues. Here, we investigate the two-photon action cross-section of CdS−CdSe−CdS segmented nanorods by extending the range of excitation from 1.55 eV (800 nm) to 0.99 eV (1250 nm). Also, the possible mechanism for the enhanced nonlinearity in heteronanostructures is elucidated on the basis of Maxwell−Garnett theory.

■ RESULTS AND DISCUSSION

The structure of CdS−CdSe−CdS segmented nanorods used in the present work is described as follows: a CdSe segment of length nearly 2 nm and diameter 4.5 nm is sandwiched between two CdS segments of nearly the same diameter as shown in the schematic (Figure 1a); the volume of a CdS segment is the same as that of the CdSe segment in the first sample (designated as sample 1-1-1), whereas it is double in the second sample (designated as sample 2-1-2).

The dimensions of the CdSe segment were monitored by analyzing the samples collected before S-TOP injection. Size distribution of the segmented nanorods was analyzed using HRTEM, shown in Figure 1b and c. The segmented nanorod structure is verified by comparing the *d*-spacing at different regions of the nanorod (Figure S1, Supporting Information). The nanorods were found to be nearly monodisperse with a diameter of 4.5 ± 0.5 nm in both samples. The total length of the segmented nanorods is determined to be 7 ± 1 nm for sample 1-1-1 (aspect ratio (AR) = 1.5) and 10 ± 1 nm for sample 2-1-2 (AR = 2.4), respectively. The selected area diffraction pattern (SAED) of the nanorods (Figure 1d) shows splitting of the diffraction peaks along different lattice directions, confirming that the CdS/CdSe interface is formed without alloying.[33] The band alignment of CdS−CdSe heteronanostructures is tunable from type I to quasi-type II and is sensitive to the dimensions of CdSe.[18] The samples were selected so that the dimensions of the CdSe segment is nearly the same, without affecting band alignment, whereas the samples can provide insight into the charge transfer and its dependence on Auger recombination.

One-photon absorption spectra of these nanorods recorded after dispersing it in toluene are shown in Figure 2a. The lowest absorption peaks observed at 2.08 eV (597 nm) for sample 1-1-1 and 2.04 eV (609 nm) for sample 2-1-2 (identified using Gaussian best fit, Figure S2, Supporting Information) are assigned as the first excitonic transition from the valence sub-bands of CdSe to the conduction sub-band of CdSe. Because of the higher volume content of CdS and its wider band gap, the absorption features at higher frequencies will be dominated by CdS. The absorption feature at 2.55 eV (486 nm) is attributed to the excitonic transitions in the CdS segments in close

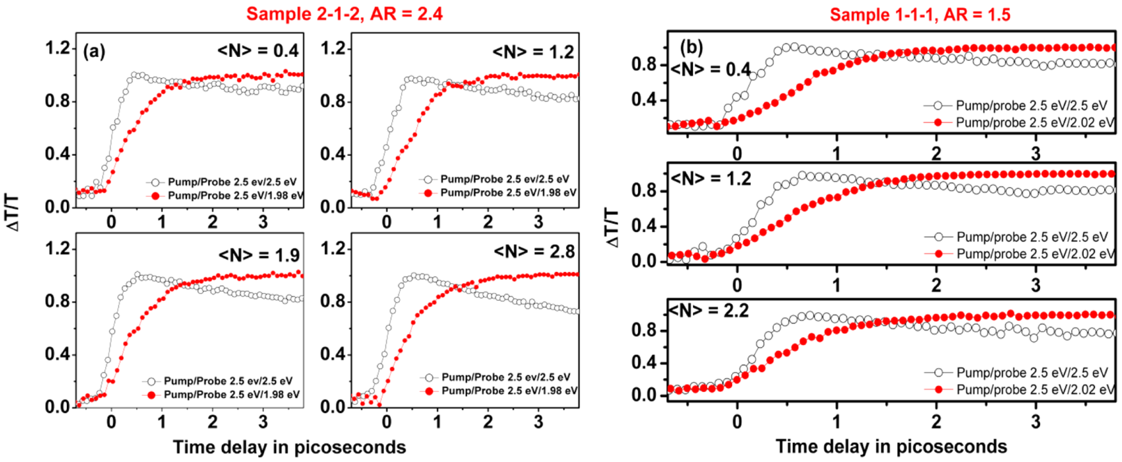

Figure 3. Transient differential transmission signal from CdS−CdSe−CdS segmented nanorods with pump at 2.5 eV (corresponding to the excitonic state of CdS) for sample 2-1-2 (a) and for sample 1-1-1 (b). Rise and decay of the charge-carrier populations can be inferred by monitoring the bleaching of the probe signal at 2.5 eV corresponding to CdS states (black, open circles) and at 1.98/2.02 eV (sample 2-1-2/sample 1-1-1) corresponding to CdSe states (red, solid circles).

proximity to the CdSe segment, where the local potential experienced is different from that of pure CdS (in the free edges of CdS segments). This observation is consistent with results obtained from other kinds of heteronanostructures of CdS−CdSe such as dot-in-rod and core−shell structures.[2,20]

The one-photon absorption induced PL in the segmented nanorods is shown in Figure 2b for different excitation wavelengths in the region from 2.1 to 3.55 eV (590 to 350 nm). The prominent emission peaks occur around 1.98 eV (625 nm) for sample 2-1-2 and around 2.02 eV (615 nm) for sample 1-1-1 irrespective of the excitation wavelength. The peaks are close to the excitonic absorption wavelengths in CdSe and are attributed to band edge emission in CdSe. A red-shift is observed in the PL emission peak of sample 1-1-1 compared to that of sample 2-1-2 (2.08 to 2.04 eV) in spite of the fact that the length and diameter of the CdSe segment are nearly the same in both samples. Such a red-shift has been reported in the case of CdS−CdSe core−shell nanoparticles and is consistent with the effective mass calculations.[2] This red-shift is attributed to the progressive delocalization of electron wave function to the CdS segments resulting in a decreased spatial confinement because of the small effective mass and negligible conduction band offset.

Weak emission bands are also seen at 2.26 eV (550 nm) as well as near 3 eV (415 nm) (inset of Figure 2b). The 2.26 eV (550 nm) emission could be arising from either the band edge emission in CdS in close proximity to CdSe or trap states in CdS.[20] The emission at 3 eV (415 nm) is attributed to the band edge emission in CdS regions near the free edges of the segmented nanorods, in the wavelength region of the band edge emission from pure CdS nanorods.[20]

The excitation wavelengths 3.5−2.5 eV (350−500 nm) are in the absorption range of CdS, whereas 2.1 eV (590 nm) is in the absorption range of CdSe. Since the emission features are basically the same for all these wavelengths of excitation, it appears that the excitons generated in the CdS segments are transferred to CdSe and subsequently undergo radiative recombination in CdSe. However, some of the excitons generated in CdS can be trapped in the defect states in CdS and eventually undergo radiative or nonradiative recombination even though the energy landscape favors the charge transfer from CdS to CdSe. Therefore, once an electron−hole (e−h) pair is generated, depending on the electronic and morphological heterogeneity, the rate of relaxation through different routes may vary. The observed emission bands corresponding to CdS at 2.99 and 2.26 eV (415 and 550 nm) are much weaker compared to the excitonic emission band in CdSe at 2.02 eV/1.98 eV (615 nm/625 nm), indicating efficient charge transfer in these systems.

PL-excitation (PLE) spectra (Figure 2c) were analyzed to provide a deeper insight into the different relaxation mechanisms in segmented nanorods. Since the emission in CdSe is a result of charge transfer from CdS, the relative quantum yield (QY) gives information about the efficiency of charge transfer. Taking into consideration the wavelength-dependent absorbance, the relative quantum yield was estimated to be 47% and 43% for sample 1-1-1 and sample 2-1-2, respectively, on excitation at 500 nm (CdS excitation) compared to that at the CdSe excitonic absorption wavelength (Figure S3, Supporting Information). In sample 1-1-1, 47% of the excitons generated in CdS are able to reach the CdSe segment, whereas nearly 43% of the excitons reach CdSe in sample 2-1-2. The rest of the carriers undergo radiative or nonradiative relaxation in CdS. This further indicates that charge transfer is efficient in these systems even when the length of the CdS segment is doubled. Increasing the aspect ratio by doubling the segment length of CdS will obviously enhance the absorption cross-section at higher energies, and the measured quantum yield supports the observation of efficient charge transfer in segmented nanorods. The dependence of PLE on the excitation energy differs in both the samples, as observable in Figure 2c, which can be understood to be due to the higher absorption cross-section at higher energies in sample 2-1-2 compared to sample 1-1-1; this in turn is a result of higher volume content of CdS in sample 2-1-2.

In order to gain further insight into the charge transfer dynamics in these segmented nanorods, we performed transient pump−probe spectroscopy, which is capable of tracking the early stages of relaxation of optically excited carriers within an ultrashort time scale (~100 fs). The pump excitation was kept at 2.5 eV, so as to excite electron−hole pairs in the CdS segments. Excitation can happen in both the CdS and CdSe segments of the nanorod at this wavelength, but the absorption is dominated by CdS, because of its higher volume content

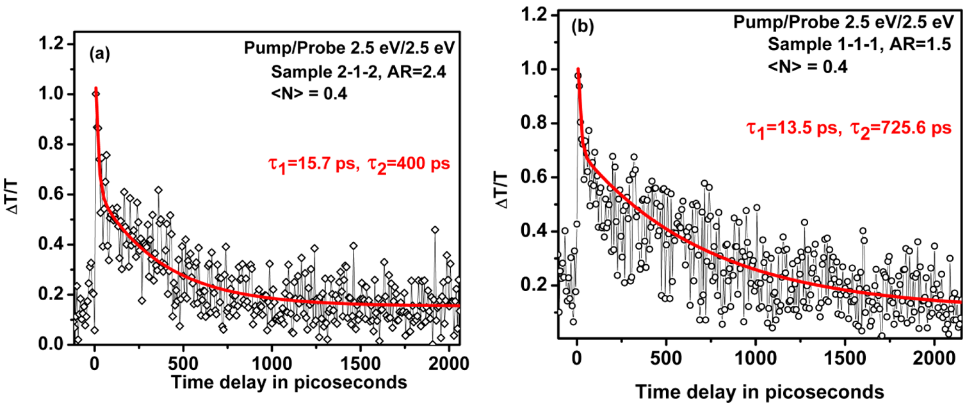

Figure 4. Transient differential transmission signal from CdS−CdSe−CdS segmented nanorods with pump and probe at 2.5 eV, corresponding to the excitonic state of CdS, in a 2 ns window for sample 2-1-2 (a) and sample 1-1-1 (b). The decay has two components, corresponding to the nonradiative and radiative transitions in CdS.

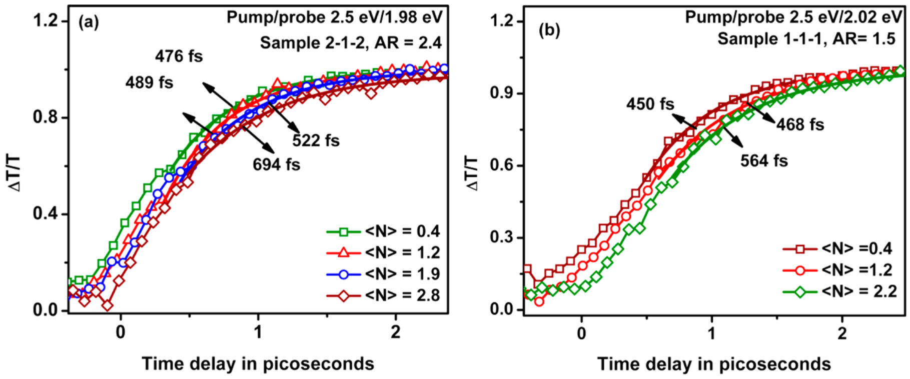

Figure 5. Transient differential transmission signal from CdS−CdSe−CdS segmented nanorods with pump at 2.5 eV, corresponding to the excitonic state of CdS, and with the probe signal at 1.98/2.02 eV (sample 2-1-2/sample 1-1-1), corresponding to CdSe states with different levels of excitation for sample 2-1-2 (a) and for sample 1-1-1 (b). The second component in the rising part of the transient was fitted with an exponential function to obtain the charge transfer rate.

compared to CdSe. Thus, the excitation at 2.5 eV predominantly creates excitons in CdS. The pump intensity is varied so that the average number of excitons generated per nanorod, denoted by $\langle N \rangle$, changes from 0.3 to 2.3. When $\langle N \rangle$ is much less than unity, the contribution of multiexcitons to the signal can be reduced. The probe energy was initially fixed at 2.5 eV to understand the dynamics in CdS and later changed to 2.02 eV (in the case of sample 1-1-1) or 1.98 eV (in the case of sample 2-1-2) to investigate the charge transfer dynamics.

Pump absorption resulting in state filling leads to an increase in transmission of the probe pulse, referred to as photobleaching, and the change in absorption is proportional to the population of the state by electrons and holes.[27,34] The time evolution of bleaching within the first few picoseconds (after excitation at 2.5 eV and probing at 2.5 and 2.02 eV/1.98 eV) is shown in Figure 3a. Monitoring the time evolution of the probe at 2.02 eV/1.98 eV after pumping at 2.5 eV can provide information about the time taken by the charge carriers to relax from the CdS segment to the CdSe segment.

The bleaching observed at the probe energy of 2.5 eV is almost instantaneous with a formation time of nearly 700 fs, which is attributed to carrier thermalization processes in CdS.[27] This is followed by a fast decay of the probe signal, indicating a decrease in population in the valence band states of CdS. Figure 3a also shows the rise of the probe signal at 2.02 eV/1.98 eV. The maximum photobleaching for this signal does not occur instantaneously, but with a time delay of nearly 2 ps. It appears that the rising part of the transient has two components, a fast and a slow component, as observed previously in CdS−CdSe core−shell structures.[25] The fast component is attributed to the intraband relaxation in CdSe. Figure 4a indicates that the rise of the slow component is in accordance with the decay of the probe signal at 2.5 eV. The photobleaching at 2.02 eV/1.98 eV is a result of an increase in population at the CdSe valence band states. Hence, the decay at 2.5 eV and the rise of the slow component at 2.02 eV/1.98 eV can be understood as occurring due to the transfer of holes from the CdS to the CdSe segment. This is possible since the potential is lower in CdSe and the band offset acts as a driving force for holes to migrate to the CdSe segment. The electrons subsequently get localized near the CdSe segment because of Coulombic attraction, leading to the formation of excitons. These excitons in CdSe recombine radiatively to give rise to PL, which explains the observed emission in these CdS−CdSe−CdS segmented nanorods.

The optically excited e−h pairs generated in the CdS segments can eventually decay through a few different pathways, of which charge transfer seems to be one of the energetically favored channels. The CdS bleaching (as seen in the decay of the probe signal at 2.5 eV) extends to long time scales up to nanoseconds, indicating that there are other possible relaxation mechanisms in CdS. This decay (shown in Figure 4a,b) can be fitted with a double-exponential function

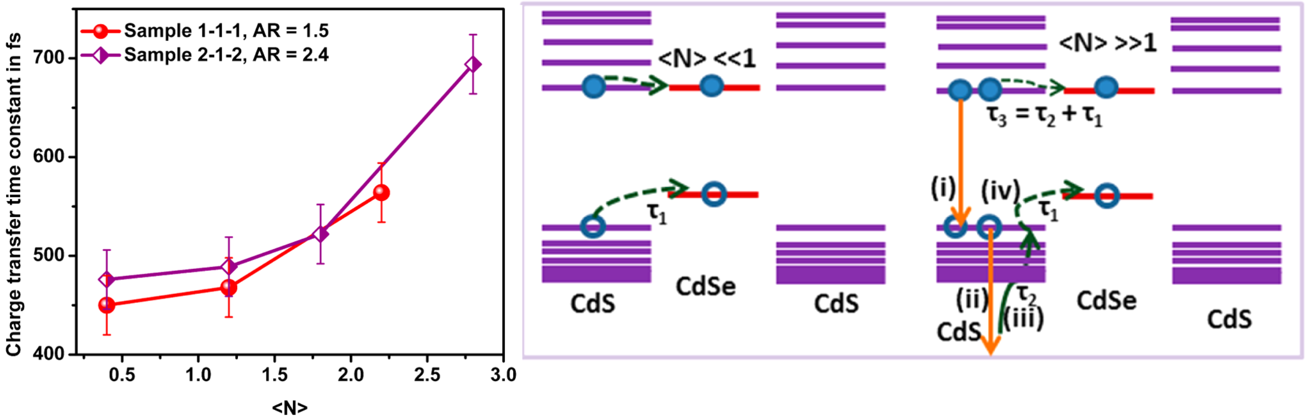

Figure 6. (a) Charge transfer time τ extracted from the exponential fit in Figure 5a and b plotted with varying $\langle N\rangle$ for CdS−CdSe−CdS segmented nanorods. (b) Schematic diagrams illustrating the charge transfer in CdS−CdSe−CdS segmented nanorods in the absence ($\langle N\rangle \ll 1$) and presence ($\langle N\rangle \gg 1$) of Auger recombination. In Auger recombination, an electron−hole pair recombines (process "i") and will exchange energy with another electron or hole, exciting it to higher energy states (process "ii"). The excited carriers undergo intraband relaxation (process "iii") with a characteristic time constant, τ_2, delaying the charge transfer from CdS to CdSe (process "iv").

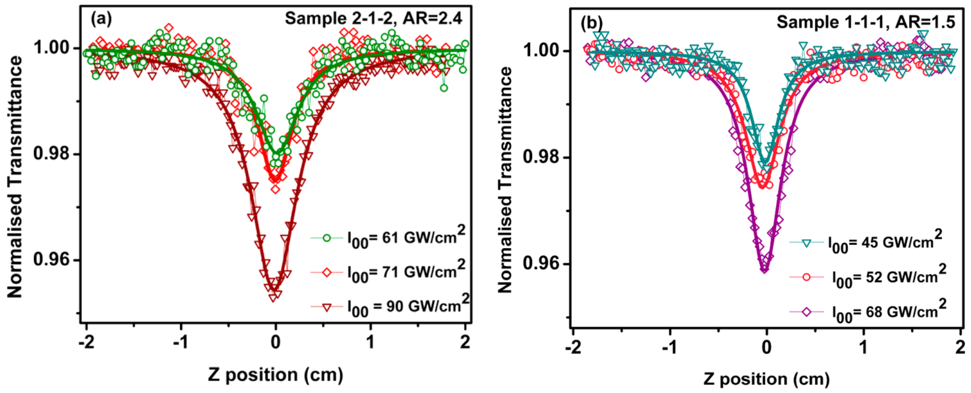

Figure 7. Open-aperture Z-scan curves obtained from CdS−CdSe−CdS segmented nanorods at 800 nm for different excitation irradiances: (a) sample 2-1-2 dispersed in toluene with a concentration of 0.5 × 10^{15} nanorods per cm^3 and (b) sample 1-1-1 dispersed in toluene with a concentration of 1 × 10^{15} nanorods per cm^3. The symbols denote the experimental data, whereas the solid lines are the Z-scan theoretical fits.

with time constants of nearly 15 and 400 ps for sample 2-1-2 and 13 and 725 ps for sample 1-1-1. These different time constants can be understood as follows: some of the generated holes may get trapped in the defect centers in the CdS segments, resulting in nonradiative decay, which corresponds to the observed time constant on the order of 10−20 ps. The holes that are trapped in the surface states may drag the electrons toward them because of the heavier hole mass and Coulombic attraction, resulting in the formation of excitons in CdS. This leads to a radiative decay, which explains the observed time constant on the order of hundreds of picoseconds. The nonradiative and radiative decay processes in CdS occur in competition with charge transfer to CdSe.

An increase in the intensity of excitation leads to an increase in carrier density, resulting in the generation of more than one e−h pair in one nanorod. Spatial confinement of the carriers to the physical dimensions of the heteronanostructure leads to forced overlap of carrier wave functions, thereby enhancing the Coulombic interaction between the excitons. This leads to annihilation of excitons by Auger recombination, which is found to be a predominant relaxation mechanism in nanocrystals. In order to investigate the effect of Auger recombination on charge transfer, we studied the charge transfer dynamics as a function of $\langle N\rangle$, which was varied by monitoring the pump intensity. The slow component in the rise time of the probe signal at 2.02 eV/1.98 eV corresponds to the hole localization time in CdSe. The rate of charge transfer can be found by an exponential fit to the slow component of the rising part of the transient from the point of inflection. Figure 5a and b show the rising transient at 2.02 eV/1.98 eV with different $\langle N\rangle$. In the case of CdS−CdSe−CdS segmented nanorods, the bleaching reaches a maximum within 2 ps after photoexcitation; this is consistent with the previous results in CdS−CdSe tetrapods.[27] The time constant for charge transfer is observed to be ∼476 fs for sample 2-1-2 and ∼450 fs for sample 1-1-1, when $\langle N\rangle \ll 1$. With nearly the same dimensions of the CdSe segment in both the samples, the valence band offset depends only on dimensions of the CdS segment. The small time constant in sample 1-1-1, compared to that in sample 2-1-2, can be understood to be due to the higher valence band offset between CdS and CdSe in the former, as a consequence of a shift in the energy levels with size variation in semiconductor nanocrystals. The charge transfer time constant was plotted with $\langle N\rangle$ in Figure 6a, which indicates that there is an increase in time constant or a decrease in the rate of charge transfer with increasing $\langle N\rangle$. The increase in time constant is quite drastic when $\langle N\rangle$ approaches a value of 2. This can be understood by correlating with the possibility of Auger recombination when $\langle N\rangle$ is greater than unity. Auger heating is known to delay the intraband relaxation process in CdSe nanorods where the biexciton lifetime is nearly 100 ps.[30] The biexciton lifetime in our segmented nanorods was also found to be on the same order (Figure S4, Supporting Information). The possible mechanism by which charge transfer could be influenced by Auger recombination is explained in the schematic shown in Figure 6b. The holes generated on optical excitation in CdS have a tendency to be transferred to CdSe. However, Auger recombination became a dominant non-radiative relaxation channel when the number of excitons generated per nanorod is greater than 1. In this relaxation mechanism, one e−h pair can recombine and give the energy to another electron or hole (process "i" in Figure 7b), exciting them to higher energy states. The excited electron can transfer the energy to the hole by e−h Coulombic interaction, which is stronger in small nanoscale structures.[29] As a result, holes get excited to higher levels within valence sub-bands (process "ii" in Figure 7b). The optically excited charge carriers created by the pump pulse would try to achieve thermal equilibrium by phonon emission. On the other hand, when $\langle N \rangle$ is greater than 1, Auger recombination results in energy release approximately equal to the energy gap, which in turn can increase the carrier temperature. The rate of energy outflow from the system by the emission of acoustic phonons will be close to the rate of increase of carrier temperature by Auger recombination in CdS and CdSe and thereby significantly alter the relaxation dynamics.[30] This additional energy received by the carriers has to be dissipated before relaxing to the ground state of CdSe, which will take additional time (process "iii" in Figure 6b). Hence, the localization of holes tends to be delayed because of Auger recombination, as explained in the proposed scheme (Figure 6b). A change in the decay (with pump and probe at 2.5 eV) is observable in the initial time scale of ∼1 ps after photoexcitation at large $\langle N \rangle$ when Auger recombination is present, supporting our proposal that the charge transfer is influenced by Auger heating (Figure S5, Supporting Information).

Our measurements indicate that the rate at which the photoexcited charge carriers in CdS get transferred to CdSe is a function of excitation intensity or in particular the average number of e−h pairs generated ($\langle N \rangle$). This indicates that the carriers are taking a longer time to cool and relax to the equilibrium state at higher $\langle N \rangle$, when Auger recombination in these nanocrystals becomes a dominant relaxation mechanism. The additional heating of carriers results in a slow rate of relaxation of carriers to equilibrium state and could affect the performance parameters (e.g., carrier mobility, switching speed) of heterojunction-based nanoscale devices. When incorporated as active component in applications such as single-photon emitters, light-emitting diodes, photovoltaic cells, lasers, and photon up-converters, knowledge of the decay dynamics of the hot and cold electron−hole (exciton) states is essential.[35] In addition to this, our studies indicate that there is a good probability of Auger recombination happening in CdS before charge transfer to CdSe, which can significantly affect the quantum yield of charge transfer from CdS to CdSe or, in other words, the luminescence efficiency when $\langle N \rangle \gg 1$. So, reducing the occurrence probability of Auger processes in CdS should also be considered while using these heteronanostructures for applications such as lasing and multiphoton microscopy since the luminescence efficiency depends on the quantum yield of charge transfer. To the best of our knowledge, this is the first observation of charge transfer being affected by Auger recombination in heteronanostructures.

One of the applications of CdS−CdSe heteronanostructures where efficient charge transfer on excitation at high intensities is important is in the field of multiphoton microscopy. In this section, we measured the spectral dependence of two-photon action cross-section of CdS−CdSe−CdS segmented nanorods by varying the excitation energy from 1.55 eV (NIR-I window) to 0.99 eV (NIR-II window). In particular, we have investigated the two-photon absorption (2PA) cross-section of the segmented nanorods at 1.55 eV (800 nm) using the Z-scan technique. Further, the two-photon action cross-section of the segmented nanorods was also determined in the range of excitation energies from 1.55 to 0.99 eV, where the two-photon action cross-section (known as the brightness of the nanorod) is defined as the product of two-photon absorption cross-section and quantum yield.

Figure 7a and b show the open-aperture Z-scans in CdS−CdSe−CdS segmented nanorods for different values of excitation irradiance, which is defined as the peak, on-axis irradiance at the focal point ($z = 0$) within the sample. The Z-scan experimental analysis is based on the assumption that $L \ll n_0 z_{0.}$[36] The nanorods were dissolved in octane with a concentration of 10^{15} nanorods per cm^3 for sample 1-1-1 and 0.5×10^{15} nanorods per cm^3 for sample 2-1-2. In our case, $L/n_0 z_0 \approx 1.6$, and hence the medium can be considered to be approximately thin and the measured 2PA coefficient is rather approximate. An analytical method was employed to find out the 2PA coefficients of the segmented nanorods.[37] The 2PA cross-section was estimated from the 2PA coefficient using the expression $\sigma_2 = (\hbar\omega\beta)/N$ where β is the 2PA coefficient, $\hbar\omega$ is the incident photon energy, and N is the concentration of nanorods in solution. The 2PA cross-section is found to be 2.4×10^4 GM for sample 1-1-1 and 4.8×10^4 GM for sample 2-1-2 at 1.55 eV (800 nm). This is comparable to the other reported heteronanostructures of CdS−CdSe of similar volume.[32]

To measure the two-photon action cross-section of the segmented nanorods in the NIR window, MPA-PL studies were conducted by varying the excitation wavelength from 800 nm to 1300 nm. The experimental details can be found elsewhere.[38] The two-photon-excited PL strength F_2 can be found by integrating Δf_2 given by $\Delta f_2 = (\eta_2 \phi \sigma_2 \rho \text{ d}s \text{ d}z \, I_r^{\,2})$, over the entire laser focused volume and time where η_2 is the PL quantum yield, ϕ is the fluorescence collection efficiency of the experimental setup, σ_2 is the two-photon absorption cross-section, ρ is the sample concentration, $\text{d}s \text{ d}z$ is the small volume of the focused laser beam considered, and I_r is the nearly constant laser intensity at this small volume.[39] By assuming Gaussian functions for the temporal and spatial profiles of input laser pulses, the total collected PL signal is given by $F_2 = (\pi^{5/2}/4)\tau\phi\eta_2\sigma_2\rho I_{00}{}^2 \omega_0{}^2 z_0$ where τ is the half-width of the Gaussian laser pulse, I_{00} is the peak intensity on the beam propagation axis, ω_0 is the beam waist, and z_0 is the diffraction length. We used rhodamine 6G molecules in methanol (0.1 mM) to calibrate our measurements. The two-photon absorption cross-section of rhodamine 6G molecule (quantum yield 0.95) is reported to be 64 GM (1 GM = 10^{-50} cm^4 s photon^{-1}) at 800 nm.[40] Then, the two-photon action cross-section of the nanorods can be obtained from the ratio of the measured PL from rhodamine 6G to the nanorods ($F_{2(\text{Rh})}/F_{2(\text{NR})} = ((\eta_2\sigma_2)_{\text{Rh}}\rho_{\text{Rh}} I_{00}{}^2)/((\eta_2\sigma_2)_{\text{NR}}\rho_{\text{NR}} I_{00}{}^2)$) where $(\eta_2\sigma_2)_{\text{Rh}}$ is known and $F_{2(\text{Rh})}$, the PL intensity, is measured at 800 nm. The action cross-section is determined to be 5.2×10^3 GM for sample 1-1-1 and 9.5×10^3 GM for sample 2-1-2. This in turn indicates that the quantum yields of sample 1-1-1 and sample 2-1-2 are nearly 21.7% and 20%, respectively. Thus, the quantum yield does not seem to change much on altering the relative volumes of CdS and CdSe segments.

Figure 8 depicts the measured spectral dependence of two-photon action cross-sections for CdS−CdSe−CdS segmented nanorods in the wavelength region from 800 to 1300 nm. The two-photon action cross-section appears to be larger for sample 2-1-2 than for sample 1-1-1 for all the wavelengths including the NIR-II window. Since the volume content of CdS for sample 2-1-2 is higher compared to sample 1-1-1, the larger two-photon action cross-section at 800 nm (the wavelength region of maximum two-photon absorption for CdS) is expected. However, the large increase in the action cross-section for sample 2-1-2 (compared to sample 1-1-1) in the low-frequency region 1050−1100 nm (NIR-II) is quite interesting. This is because CdSe is expected to contribute toward two-photon absorption in this wavelength range (1.1 eV) and the volume of CdSe remains the same in both the samples. This implies that the volume of CdS also matters in these nanocomposites in determining the two-photon absorption. In the following, we attempt to use Maxwell−Garnett theory, which has been widely used to explain and predict the optical nonlinearity in composite materials[41,42] to account for the observations.

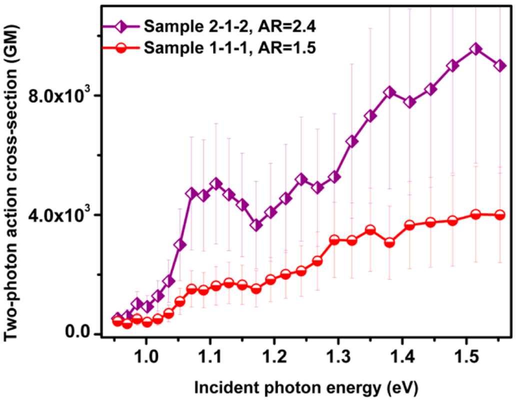

Figure 8. Two-photon action cross-section estimated for CdS−CdSe−CdS segmented nanorods in the range of incident photon energy 0.95 to 1.55 eV.

According to this theory, a composite can be viewed as a homogeneous medium with effective optical parameters, such as effective dielectric constant or effective linear and nonlinear susceptibilities, which are related to the optical parameters of the individual constituents. Here a composite is defined as any material made up of two or more different constituents with size or dimensions much less than the optical wavelength. Maxwell−Garnett theory was originally proposed for predicting/explaining the enhancement in the nonlinear susceptibility of semiconductor inclusions in glass. As stated by the theory, the electric field driving the polarization in the inclusion particle, defined as the local field, depends not only on the applied field but also on the polarization of the surrounding medium.[41] Because of this redistribution of the electric field in composites, the optical constants are not just the weighted averages of the optical constants of constituents. The significance of local field is quite large in the calculation of third-order susceptibility since it depends on the fourth power of the local field correction factor.[41] Recently, Maxell−Garnett theory was extended to explain the one-photon absorption in core−shell heteronanostructures.[43,44] The local field factor in the core of a core−shell nanoparticle depends on the ratio of the volume of the shell to the total volume of the core−shell as per the relation $f_{\mathrm{LF}} = 9\varepsilon_{\mathrm{sh}}\varepsilon_{\mathrm{s}}/(\varepsilon_{\mathrm{sh}}\varepsilon_{\mathrm{a}} + 2\varepsilon_{\mathrm{s}}\varepsilon_{\mathrm{b}})$ where $\varepsilon_{\mathrm{a}} = \varepsilon_{\mathrm{c}}(3 - 2(V_{\mathrm{sh}}/V_{\mathrm{QD}})) + 2\varepsilon_{\mathrm{sh}}(V_{\mathrm{sh}}/V_{\mathrm{QD}})$ and $\varepsilon_{\mathrm{b}} = \varepsilon_{\mathrm{c}}(V_{\mathrm{sh}}/V_{\mathrm{QD}}) + \varepsilon_{\mathrm{sh}}(3 - (V_{\mathrm{sh}}/V_{\mathrm{QD}}))$. This is a result of the change in effective dielectric constant and not due to a quantum confinement effect. This implies that addition of a shell can alter significantly the optical constants of the core material. Applying this theory to the segmented nanorod structure, it can be expected that the local field experienced in CdSe depends also on the volume of CdS present in the segmented nanorod structure. The volume ratio of CdS to CdSe is nearly 0.8 in sample 2-1-2, whereas that in sample 1-1-1 is 0.667. So, the local field experienced in CdSe can be modified significantly by the amount of CdS. This change in local field can effectively alter the third-order susceptibility and, hence, the two-photon absorption coefficient. The segmented nanorods used in the present work are dispersed in toluene, a linear medium in the wavelength of interest. In this case, the third-order susceptibility depends on the fourth power of the local field factor. The ratio of the fourth power of the local field in sample 2-1-2 to that in sample 1-1-1 was calculated to be 1.15, indicating an enhancement of 1.15 in the NIR-II region. The measured enhancement factor from the experimental results is found to be nearly 2, in close agreement with the theoretical prediction. This enhancement can therefore be understood to be due to the modification of the electric field distribution in CdSe in the presence of CdS.

A few factors other than the local field effect could also influence the enhancement in the nonlinear absorption coefficient of CdS−CdSe. The segmented nanorods have Wurtzite structure, which has an intrinsic dipole moment and polarization along the *c* crystallographic axis, resulting from the deviation from the ideal wurtzite structure, quite unavoidable in real wurtzite structures. This intrinsic dipole moment is known to scale linearly with volume,[45] which would affect the enhancement factor. Also, the radiative surface states can trap holes, with the electron still being delocalized as a result of reduced effective mass, leading to a reduced electron−hole overlap and a permanent dipole moment.[46] The intrinsic dipole moment as well as the photoinduced dipole moment due to surface states will be larger in sample 2-1-2 than in sample 1-1-1, thereby explaining the enhanced nonlinearity. Our studies indicate that the nature of nonlinearity in heteronanostructures can be engineered by varying factors such as volume of the constituent materials and the effective dielectric constant, thus offering a platform for a wide range of applications.

■ CONCLUSION

We report on the influence of Auger recombination on the charge transfer of photoexcited carriers in CdS−CdSe−CdS segmented nanorods. The chosen segmented nanorod offers an advantage of the possibility of varying the relative volumes of the individual segments, thereby providing a control of the absorption cross-section over a wide range of wavelengths. Transient pump−probe experiments reveal that the rate of charge transfer depends on the number of electron−hole pairs generated per nanorod ($\langle N\rangle$), causing a delay in hole localization in CdSe with increase in $\langle N\rangle$, the effect becoming prominent as $\langle N\rangle$ approaches 2. This could be due to enhanced carrier−carrier interaction when $\langle N\rangle \gg 1$, resulting in Auger recombination. This leads to an additional heating of carriers, requiring additional time for energy dissipation before localization. The observation of the influence of Auger recombination on charge transfer in heteronanostructures has technological implications. Charge transfer in these nanostructures also leads to two-photon absorption induced PL on NIR excitation. Our studies indicate that local field effects in the individual components of a heteronanostructure can play a significant role in their nonlinear optical response, thus offering a platform for the design of optoelectronic devices based on heteronanostructures with controllable parameters of operation.

EXPERIMENTAL DETAILS

Synthesis. Ethanol (99.9%, Emisure), *n*-hexane (99.7%, J. T. Baker), cadmium oxide (CdO, 99.95%, Alfa Aesar), sulfur sublimed (S, 99.65%, Chemicon), selenium metal (Se, 99.9%, Fluka), 1-tetradecylphosphonic acid (TDPA, 98%, Alfa Aesar), trioctylphosphine oxide (TOPO, 99%, Aldrich), and tri-*n*-octylphosphine (TOP, 90%, Alfar Aesar) were used directly without any prior purification.

Synthesis of the nanorods followed a method adopted from Korgel.[47] Stock solutions were first prepared. Cd precursor was prepared by adding 0.0342 g of CdO, 0.1290 g of TDPA, and 2.1000 g of TOPO into a three-necked round-bottom flask. The reaction mixture was degassed at 65 °C for 3 h and subsequently heated to 340 °C under an inert environment for 10 min. The S-TOP and Se-TOP stock solutions were prepared by dissolving 0.0064 g of S and 0.0158 g of Se separately in 1 mL of TOP and heating them to 120 °C under an inert environment until the solution became homogeneous (~5 min). To obtain CdS−CdSe−CdS (1:1:1) nanorods, the Cd precursor mixture was first lowered to 260 °C and 2 × 0.1 mL of Se-TOP was injected in 3 min intervals. After that, the temperature was raised to 300 °C, followed by 4 × S-TOP injections of 0.1 mL 2 min apart. For the CdS−CdSe−CdS (2:1:2) nanorods, the procedure was exactly the same except that 8 × S-TOP injections of 0.1 mL were performed. After the final injection, the reaction mixture was allowed to react for another 10 min before cooling to room temperature under an inert atmosphere. The products were precipitated from the crude mixture using ethanol, centrifuged, and subsequently redispersed into hexane for further study.

One-Photon Spectroscopy Measurements. One-photon absorption spectra of CdS−CdSe−CdS segmented nanorods were acquired using a UV−visible−near IR spectrophotometer (Shimadzu, UV-1700), and one-photon-absorption-induced PL spectra were collected with a Jasco FP-6300 spectrofluorometer.

Transient Pump−Probe Spectroscopy. The laser pulses with tunable wavelength (300−1600 nm, 150 fs, 1 kHz) were produced by a mode-locked Ti:Sapphire laser seeded Ti:Sapphire regenerative amplifier (Coherent, Vitesse) pumped OPA (TOPAS). For pump−probe experiments, the signal beam at 800 nm and the output from the OPA were spatially and temporally overlapped in a BBO crystal for sum frequency generation, and an appropriate filter was used at the output. The laser pulse width of 150 fs allows us to detect the signals corresponding to charge transfer, which happens within some picoseconds after photoexcitation. The schematic diagram showing the experimental setup can be found elsewhere.[48] In this experiment, the pump and probe pulses were orthogonally polarized with the incident angle between both the beams less than three degrees. The ratio of energy between the pump and the probe pulses was less than 5%.

Z-Scan Technique. For the Z-scan experiment, the laser pulses (800 nm, 150 fs, 1 kHz) from the above-mentioned laser system were used. The 1 kHz repetition rate eliminates or minimizes the thermal contribution to the measured 2PA coefficient. The laser beam was focused into the sample to a minimum beam waist of nearly 25 μm by means of a 10 cm focal length lens. The details of the Z-scan technique can be found elsewhere.[37] The solutions of sample 1-1-1 or 2-1-2 were contained in 1 cm thick quartz cells for the Z-scans. In this open aperture (OA) Z-scan technique, the total transmitted energy in the far field was measured as a function of sample position.

Multiphoton-Absorption-Induced PL Studies. The two-photon absorption induced PL emission from CdS−CdSe−CdS segmented nanorods was studied in the range from 1.55 to 0.99 eV (800 to 1250 nm). The incident laser pulses from the OPA (800−1300 nm, 150 fs, 1 kHz) were focused by a 10 cm focal length lens onto a 1 cm thick quartz cell containing the solution of sample 1-1-1 or 2-1-2. The laser beam was focused into the solution by means of a lens of focal length 10 cm, and the beam spot size at the focal plane was 26−28 μm. The multiphoton-excited PL signal was collected in the perpendicular direction of the incident light using a collection system of two 10 cm focal length lenses and then coupled into a spectrometer (Avaspec- 2048-SPU, resolution 0.5 nm). As a calibration, a standard sample, rhodamine 6G, which shows quadratic dependence on excitation fluence at 800 nm, was employed in the same experimental setup.

ASSOCIATED CONTENT

Ⓢ Supporting Information

Figure S1, Determination of the segmented nanorod structure by identifying the *d*-spacing at three different regions of the nanorod. Figure S2, Gaussian fitting of UV−visible absorption data. Figure S3, Quantum yield of charge transfer from CdS to CdSe. Figure S4, Intensity-dependent decay observed with pump and probe at 2.5 eV. Figure S5, Change in the decay observed with pump and probe at 2.5 eV during the initial time scale after photoexcitation, supporting our proposal that Auger recombination is happening at ~1 ps. This material is available free of charge via the Internet at http://pubs.acs.org.

AUTHOR INFORMATION

Corresponding Author

*E-mail: phyjiwei@nus.edu.sg.

Notes

The authors declare no competing financial interest.

REFERENCES

(1) Chen, O.; Zhao, J.; Chauhan, V. P.; Cui, J.; Wong, C.; Harris, D. K.; Wei, H.; Han, H.-S.; Fukumura, D.; Jain, R. K.; Bawendi, M. G. Compact high-quality CdSe−CdS core−shell nanocrystals with narrow emission linewidths and suppressed blinking. *Nat. Mater.* **2013**, *12*, 445−451.

(2) García-Santamaría, F.; Brovelli, S.; Viswanatha, R.; Hollingsworth, J. A.; Htoon, H.; Crooker, S. A.; Klimov, V. I. Breakdown of volume scaling in Auger recombination in CdSe/CdS heteronanocrystals: the role of the core−shell interface. *Nano Lett.* **2011**, *11*, 687−693.

(3) Grivas, C.; Li, C.; Andreakou, P.; Wang, P.; Ding, M.; Brambilla, G.; Manna, L.; Lagoudakis, P. Single-mode tunable laser emission in the single-exciton regime from colloidal nanocrystals. *Nat. Commun.* **2013**, *4*.

(4) García-Santamaría, F.; Chen, Y.; Vela, J.; Schaller, R. D.; Hollingsworth, J. A.; Klimov, V. I. Suppressed Auger recombination in "giant" nanocrystals boosts optical gain performance. *Nano Lett.* **2009**, *9*, 3482−3488.

(5) Htoon, H.; Malko, A. V.; Bussian, D.; Vela, J.; Chen, Y.; Hollingsworth, J. A.; Klimov, V. I. Highly emissive multiexcitons in steady-state photoluminescence of individual "giant" CdSe/CdS core/shell nanocrystals. *Nano Lett.* **2010**, *10*, 2401−2407.

(6) Talapin, D. V.; Nelson, J. H.; Shevchenko, E. V.; Aloni, S.; Sadtler, B.; Alivisatos, A. P. Seeded growth of highly luminescent CdSe/CdS nanoheterostructures with rod and tetrapod morphologies. *Nano Lett.* **2007**, *7*, 2951−2959.

(7) Dai, M.-Q.; Zheng, W.; Huang, Z.; Lanry Yung, L.-Y. Aqueous phase synthesis of widely tunable photoluminescence emission CdTe/CdS core/shell quantum dots under a totally ambient atmosphere. *J. Mater. Chem.* **2012**, *22*, 16336−16345.

(8) Lee, Y.-b.; Park, S.; Lee, S.; Kim, J.; Lee, K.-S.; Joo, J. Nanoscale luminescence characteristics of CdSe/ZnS quantum dots hybridized

with organic and metal nanowires: energy transfer effects. *J. Mater. Chem. C* **2013**, *1*, 2145−2151.

(9) Zhong, X.; Xie, R.; Zhang, Y.; Basché, T.; Knoll, W. High-quality violet- to red-emitting ZnSe/CdSe core/shell nanocrystals. *Chem. Mater.* **2005**, *17*, 4038−4042.

(10) Ivanov, S. A.; Piryatinski, A.; Nanda, J.; Tretiak, S.; Zavadil, K. R.; Wallace, W. O.; Werder, D.; Klimov, V. I. Type-II Core/Shell CdS/ZnSe nanocrystals: synthesis, electronic structures, and spectroscopic properties. *J. Am. Chem. Soc.* **2007**, *129*, 11708−11719.

(11) Pal, B. N.; Ghosh, Y.; Brovelli, S.; Laocharoensuk, R.; Klimov, V. I.; Hollingsworth, J. A.; Htoon, H. 'Giant' CdSe/CdS core/shell nanocrystal quantum dots as efficient electroluminescent materials: strong influence of shell thickness on light-emitting diode performance. *Nano Lett.* **2011**, *12*, 331−336.

(12) Wen, X.; Sitt, A.; Yu, P.; Toh, Y.-R.; Tang, J. Temperature dependent spectral properties of type-I and quasi type-II CdSe/CdS dot-in-rod nanocrystals. *Phys. Chem. Chem. Phys.* **2012**, *14*, 3505−3512.

(13) Rainò, G.; Stöferle, T.; Moreels, I.; Gomes, R.; Kamal, J. S.; Hens, Z.; Mahrt, R. F. Probing the wave function delocalization in CdSe/CdS dot-in-rod nanocrystals by time- and temperature-resolved spectroscopy. *ACS Nano* **2011**, *5*, 4031−4036.

(14) Lutich, A. A.; Mauser, C.; Da Como, E.; Huang, J.; Vaneski, A.; Talapin, D. V.; Rogach, A. L.; Feldmann, J. Multiexcitonic Dual Emission in CdSe/CdS Tetrapods and Nanorods. *Nano Lett.* **2010**, *10*, 4646−4650.

(15) Scotognella, F.; Miszta, K.; Dorfs, D.; Zavelani-Rossi, M.; Brescia, R.; Marras, S.; Manna, L.; Lanzani, G.; Tassone, F. Ultrafast exciton dynamics in colloidal CdSe/CdS octapod shaped nanocrystals. *J. Phys. Chem. C* **2011**, *115*, 9005−9011.

(16) Zhang, Y.; Miszta, K.; Manna, L.; Di Fabrizio, E.; Krahne, R. Cold field emission dominated photoconductivity in ordered three-dimensional assemblies of octapod-shaped CdSe/CdS nanocrystals. *Nanoscale* **2013**, *5*, 7596−7600.

(17) Cassette, E.; Mahler, B.; Guigner, J.-M.; Patriarche, G.; Dubertret, B.; Pons, T. Colloidal CdSe/CdS dot-in-plate nanocrystals with 2D-polarized emission. *ACS Nano* **2012**, *6*, 6741−6750.

(18) Sitt, A.; Sala, F. D.; Menagen, G.; Banin, U. Multiexciton engineering in seeded core/shell nanorods: transfer from type-I to quasi-type-II regimes. *Nano Lett.* **2009**, *9*, 3470−3476.

(19) Borys, N. J.; Walter, M. J.; Huang, J.; Talapin, D. V.; Lupton, J. M. The role of particle morphology in interfacial energy transfer in CdSe/CdS heterostructure nanocrystals. *Science* **2010**, *330*, 1371−1374.

(20) Wu, K.; Rodríguez-Córdoba, W. E.; Liu, Z.; Zhu, H.; Lian, T. Beyond band alignment: hole localization driven formation of three spatially separated long-lived exciton states in CdSe/CdS nanorods. *ACS Nano* **2013**, *7*, 7173−7185.

(21) Giblin, J.; Kuno, M. Nanostructure absorption: a comparative study of nanowire and colloidal quantum dot absorption cross sections. *J. Phys. Chem. Lett.* **2010**, *1*, 3340−3348.

(22) Hu, J.; Li, L.-s.; Yang, W.; Manna, L.; Wang, L.-w.; Alivisatos, A. P. Linearly polarized emission from colloidal semiconductor quantum rods. *Science* **2001**, *292*, 2060−2063.

(23) Prasankumar, R. P.; Upadhya, P. C.; Taylor, A. J. Ultrafast carrier dynamics in semiconductor nanowires. *Phys. Status Solidi B* **2009**, *246*, 1973−1995.

(24) Othonos, A. Probing ultrafast carrier and phonon dynamics in semiconductors. *J. Appl. Phys.* **1998**, *83*, 1789−1830.

(25) Schill, A. W.; Gaddis, C. S.; Qian, W.; El-Sayed, M. A.; Cai, Y.; Milam, V. T.; Sandhage, K. Ultrafast electronic relaxation and charge-carrier localization in CdS/CdSe/CdS quantum-dot quantum-well heterostructures. *Nano Lett.* **2006**, *6*, 1940−1949.

(26) Lupo, M.; Carbone, L.; Manna, L.; Cingolani, R.; Zavelani-Rossi, M.; Lanzani, G., Ultrafast carrier dynamics in spherical CdSe core/elongated CdS shell nanocrystals. In *Ultrafast Phenomena XVI*; Corkum, P.; Silvestri, S.; Nelson, K. A.; Riedle, E.; Schoenlein, R. W., Eds.; Springer: Berlin, 2009; Vol. *92*, pp 289−291.

(27) Mauser, C.; Da Como, E.; Baldauf, J.; Rogach, A. L.; Huang, J.; Talapin, D. V.; Feldmann, J. Spatio-temporal dynamics of coupled electrons and holes in nanosize CdSe−CdS semiconductor tetrapods. *Phys. Rev. B* **2010**, *82*, 081306.

(28) Lupo, M. G.; Della Sala, F.; Carbone, L.; Zavelani-Rossi, M.; Fiore, A.; Lüer, L.; Polli, D.; Cingolani, R.; Manna, L.; Lanzani, G. Ultrafast electron−hole dynamics in core/shell CdSe/CdS dot/rod nanocrystals. *Nano Lett.* **2008**, *8*, 4582−4587.

(29) Klimov, V. I.; Mikhailovsky, A. A.; McBranch, D. W.; Leatherdale, C. A.; Bawendi, M. G. Quantization of multiparticle Auger rates in semiconductor quantum dots. *Science* **2000**, *287*, 1011−1013.

(30) Achermann, M.; Bartko, A. P.; Hollingsworth, J. A.; Klimov, V. I. The effect of Auger heating on intraband carrier relaxation in semiconductor quantum rods. *Nat. Phys.* **2006**, *2*, 557−561.

(31) Xing, G.; Liao, Y.; Wu, X.; Chakrabortty, S.; Liu, X.; Yeow, E. K. L.; Chan, Y.; Sum, T. C. Ultralow-threshold two-photon pumped amplified spontaneous emission and lasing from seeded CdSe/CdS nanorod heterostructures. *ACS Nano* **2012**, *6*, 10835−10844.

(32) Allione, M.; Ballester, A.; Li, H.; Comin, A.; Movilla, J. L.; Climente, J. I.; Manna, L.; Moreels, I. Two-photon-induced blue shift of core and shell optical transitions in colloidal CdSe/CdS quasi-type II quantum rods. *ACS Nano* **2013**, *7*, 2443−2452.

(33) Ouyang, L.; Maher, K. N.; Yu, C. L.; McCarty, J.; Park, H. Catalyst-assisted solution−liquid−solid synthesis of CdS/CdSe nanorod heterostructures. *J. Am. Chem. Soc.* **2006**, *129*, 133−138.

(34) Klimov, V. I. Optical nonlinearities and ultrafast carrier dynamics in semiconductor nanocrystals. *J. Phys. Chem. B* **2000**, *104*, 6112−6123.

(35) Hendry, E.; Koeberg, M.; Wang, F.; Zhang, H.; de Mello Donegá, C.; Vanmaekelbergh, D.; Bonn, M. Direct observation of electron-to-hole energy transfer in CdSe quantum dots. *Phys. Rev. Lett.* **2006**, *96*, 057408.

(36) Sheik-Bahae, M.; Said, A. A.; Wei, T. H.; Hagan, D. J.; Van Stryland, E. W. Sensitive measurement of optical nonlinearities using a single beam. *IEEE J. Quantum Electron.* **1990**, *26*, 760−769.

(37) He, J.; Qu, Y.; Li, H.; Mi, J.; Ji, W. Three-photon absorption in ZnO and ZnS crystals. *Opt. Express* **2005**, *13*, 9235−9247.

(38) Subha, R.; Nalla, V.; Yu, J. H.; Jun, S. W.; Shin, K.; Hyeon, T.; Vijayan, C.; Ji, W. Efficient photoluminescence of Mn^{2+}-doped ZnS quantum dots excited by two-photon absorption in near-infrared window II. *J. Phys. Chem. C* **2013**, *117*, 20905−20911.

(39) Xing, G.; Ji, W.; Zheng, Y.; Y. Ying, J. High efficiency and nearly cubic powerdependence of below-band-edge photoluminescence in water-soluble, copperdoped ZnSe/ZnS Quantum dots. *Opt. Express* **2008**, *16*, 5715−5720.

(40) Makarov, N. S.; Drobizhev, M.; Rebane, A. Two-photon absorption standards in the 550−1600 nmexcitation wavelength range. *Opt. Express* **2008**, *16*, 4029−4047.

(41) Gehr, R. J.; Boyd, R. W. Optical properties of nanostructured optical materials. *Chem. Mater.* **1996**, *8*, 1807−1819.

(42) Huang, J. P.; Yu, K. W. Enhanced nonlinear optical responses of materials: composite effects. *Phys. Rep.* **2006**, *431*, 87−172.

(43) De Geyter, B.; Hens, Z. The absorption coefficient of PbSe/CdSe core/shell colloidal quantum dots. *Appl. Phys. Lett.* **2010**, *97*, 161908.

(44) Neeves, A. E.; Birnboim, M. H. Composite structures for the enhancement of nonlinear-optical susceptibility. *J. Opt. Soc. Am. B* **1989**, *6*, 787−796.

(45) Li, L.-s.; Alivisatos, A. P. Origin and scaling of the permanent dipole moment in CdSe nanorods. *Phys. Rev. Lett.* **2003**, *90*, 097402.

(46) Wang, Y. Nonlinear optical properties of nanometer-sized semiconductor clusters. *Acc. Chem. Res.* **1991**, *24*, 133−139.

(47) Shieh, F.; Saunders, A. E.; Korgel, B. A. General shape control of colloidal CdS, CdSe, CdTe quantum rods and quantum rod heterostructures. *J. Phys. Chem. B* **2005**, *109*, 8538−8542.

(48) Yang, H.; Feng, X.; Wang, Q.; Huang, H.; Chen, W.; Wee, A. T. S.; Ji, W. Giant two-photon absorption in bilayer graphene. *Nano Lett.* **2011**, *11*, 2622−2627.